MOVING TARGET DEPTH ESTIMATION FOR PASSIVE SONAR, USING SEQUENTIAL RESAMPLING TECHNIQUES

Shawn Kraut and Jeffrey Krolik

Dept. of ECE, Box 90291
Duke University
Durham, NC 27708-0291
kraut@ee.duke.edu, jk@ee.duke.edu

ABSTRACT

We examine the problem of passive localization of a moving target in a littoral environment, based on its depth and range-rate. We compare performance with the conventional matched field processor, which localizes in depth and range. Range-rate localization is more robust with respect to uncertainties in the environment, and with respect to associated uncertainties in the horizontal wave numbers of the channel modes used for the matched field target response. In our approach the complex amplitudes of the modes are treated as nuisance parameters, which comprise a hidden, first-order Markov state process. In lieu of an analytic expression for the evolution of the likelihood function as new snapshots are integrated, we evaluate a method of particle filtering, or sequential resampling.

1. INTRODUCTION

Matched field processing (MFP) techniques localize targets in shallow water environments by computing a replica vector based on channel modes associated with a given set of environmental parameters, including the sound-speed profile [3]. They typically suffer from high sidelobes and ambiguous peaks produced at ambiguous ranges and depths, a problem that is exacerbated by environmental uncertainties. Modifications to the MVDR beamformer have been proposed to make it more robust to these uncertainties, by constraining the weight vector to stabilize its response over an ensemble of environments [1]. An additional problem is target motion, which spreads the target peak, decreasing its visibility. Previous work on target motion has focused on applying a transformations to successive data snapshots that compensate for motion corresponding to a particular hypothesized velocity, resulting in a focused peak in the range-depth ambiguity surface for a target having that velocity [2]. The main idea of this paper is to view target

motion as an asset rather than a liability, and to jointly estimate depth and range-rate in a manner that not only compensates for target motion, but also enhances robustness to environmental uncertainty. We propose to implement this by constructing a state model for the replica vector, using an assumed target velocity to constrain the state evolution, and leaving the initial state, which depends on target range, as a nuisance parameter. Because we do not have a closed-form, analytic solution for the updating of the likelihood function that arises from this state model, we instead examine a non-parametric method of approximating the likelihood, a sequential resampling or "particle filtering" method [4, 5].

2. MATCHED FIELD PROCESSING

Matched field processing obtains a replica vector for a target in shallow water based on the Green's function for the target response. For a shallow water environment, the response at the nth sensor can be expanded in terms of the eigenmodes of the channel as follows [6, 7]:

$$s_k(n) = \sum_{m=1}^{M} \sqrt{\frac{2\pi}{k_r(m)r}} \psi_m(c_n)\psi_m(d) \exp(-j\, k_r(m) \cdot r).$$

$$(1)$$

Here k, m, and n index the time of the snapshot, the mode number, and the array sensor number, respectively. The sum is over the M eigenmodes $\psi_m(z)$ supported by the channel, where z is the depth coordinate. The eigenmodes are sampled at c_n, the depth of the nth sensor, and at d, the depth of the target. The amplitude of the mth mode includes a phase factor proportional to the product of its horizontal wave number $k_r(m)$ and the target range r. Rewriting this expression in terms of the N-dimensional replica vector $\underline{s}_k$, where N is the number of hydrophone sensors, we have:

$$\underline{s}_k(d,r) = \Psi(\underline{c})[\underline{\phi}(d,r) \odot \underline{x}_k(r)], \qquad (2)$$

where $\odot$ denotes the Hadamard, or element-by-element, vector product. Here the nth element of $\underline{s}_k$ is $s_k(n)$, the (n,m)

20020807 242

element of $\boldsymbol{\Psi}$ is $\psi_m(c_n)$, and the mth element of $\underline{\phi}(d, r)$ is $\sqrt{\frac{2\pi}{k_r(m)r}}\psi_m(d)$. The modal phases have been collected into a vector $\underline{x}_k(r)$, whose m^{th} element is given by $\exp(-j\ k_r(m)) \cdot r)$.

If the target is presumed to be stationary, so that the replica vector is constant across a window of K snapshots, $\underline{s}_k = \underline{s}$, then summing over the matched-filter output of K snapshots yields the conventional matched field processor, or Bartlett estimate [8]:

$$\frac{1}{K} \sum_{k=1}^{K} \frac{\|\underline{s}^\dagger \underline{y}_k\|^2}{\underline{s}^\dagger \underline{s}} = \frac{\underline{s}^\dagger \hat{\mathbf{R}}_{yy} \underline{s}}{\underline{s}^\dagger \underline{s}}, \qquad (3)$$

where $\hat{\mathbf{R}}_{yy} = \frac{1}{K} \sum_k \underline{y}_k \underline{y}_k^\dagger$, is the sample correlation matrix of the data.

This estimator is also justified by the likelihood of the data, as a function of depth d and range r, over the window of snapshots, if the data has the random model $\underline{y}_k = a_k\underline{s} + \underline{n}_k$. Here the signal has a Gaussian distributed complex amplitude $a_k \sim CN[0, \sigma_s^2]$, and there is additive white measurement noise $\underline{n}_k \sim CN[\underline{0}, \sigma_n^2\mathbf{I}]$. Then by using Woodbury identities (a brief derivation is reproduced in in Appendix 3.7 of [9]), the likelihood of the kth snapshot can be shown to be

$$f(\underline{y}_k|\underline{s}(d, r)) = \frac{1}{(\pi\sigma^2)^N \left(1 + \frac{\sigma_s^2}{\sigma_n^2}\underline{s}^\dagger\underline{s}\right)}$$

$$\cdot \exp\left\{-\frac{\underline{y}_k^\dagger\underline{y}_k}{\sigma_n^2} + \frac{\|\underline{s}^\dagger\underline{y}_k\|^2}{\sigma_n^2\left(\frac{\sigma_n^2}{\sigma_s^2} + \underline{s}^\dagger\underline{s}\right)}\right\}. \qquad (4)$$

Conditioned on $\underline{s}$, all the data vectors $\underline{y}_k$ are independent and share the same likelihood. In the high SNR limit, $\sigma_s^2 \gg \sigma_n^2$, their joint log-likelihood, as a function of (d, r), is proportional to the Bartlett estimate of Equation 3.

An alternative approach, the MVDR beamformer or Capon spectrum, has advantages for suppressing interfering sources and sidelobes. However it is more sensitive to target nulling if the presumed target replica vector is mismatched with respect to the true target response. In this work we investigate robustness with respect to errors in environmental parameters, which can produce target mismatch. We evaluate our Moving Target Depth Estimator (MTDE) and the Bartlett estimator, or conventional matched field processor, as a baseline estimator for comparison.

3. TARGET MOTION, ENVIRONMENTAL MISMATCH, AND DEPTH AMBIGUITY

Two phenomenon which degrade the performance of the Bartlett estimator are target motion and environmental mismatch. Here we examine the scenario in which a target is moving in range at a constant velocity and constant depth. Target motion tends to smear out the peak target power across range, reducing peak height and the effective post-beamformer SNR. An example realization of an ambiguity surface is shown in Figure 1, where the target has moved from 10 to 10.5 km over 50 snapshots spaced two seconds apart, as indicated by the white line segment bounded by stars. Note that there are ambiguous peaks at other ranges at the same depth as the target (20m), but also at a depth of about 83m. (The cause of the ambiguous depth will be discussed below.)

Environmental mismatch produces mismatch of the replica vector $\underline{s}$. The replica vector is a function of both range and depth, but it is range localization that seems to be more seriously affected by mismatch, as shown in Figure 2. To understand this, consider Equation 2. The depth dependence is contained in the vector $\underline{\phi}$, the mode amplitudes sampled at the source depth. This vector also has a global scaling inversely proportional to range; the average range effectively scales the signal power σ_s^2. The primary dependence on range is contained the vector of modal phases $\underline{x}_k$, each phase being proportional to the product of the horizontal wavenumber and the range, $k_r(m) \cdot r$. A small mismatch in the wavenumber $k_r(m)$ can cause a big mismatch in the phase, as it is multiplied by a range r than can be on the order of several kilometers.

Our initial investigation of environmental mismatch is based on the simple Pekeris model, with a uniform soundspeed in the water channel, and in the ocean bottom [6, 7]. Mismatch is implemented by using the Pekeris model to generate synthetic data, then perturbing the vertical wavenumbers k_z assumed in processing the data and forming an ambiguity surface. The wavenumbers are perturbed by a uniform random variable whose extent we express as a fraction of $\frac{pi}{h}$, the approximate spacing of the vertical wavenumbers, where $h = 100m$ is the depth of the water column. Then the assumed modes $\psi_m(z)$ and horizontal wavenumbers $k_r = \sqrt{k_0^2 - k_z^2}$ are computed accordingly. For example, in Figure 2, they are perturbed by $\pm 4.5\frac{\pi}{h}$, the total range of the perturbations being $0.9\frac{\pi}{h}$. Note that while the range information has been lost, there is still significant energy distributed, across several ranges, at the correct depth of 20m and at an ambiguous depth of about 83.5 m

To see the source of the depth ambiguity, refer to Figure 3, in which we plot $\underline{\phi}(d)$ at $d = 20m$ and $d = 83.5m$, as well as the magnitude of $\underline{\phi}(d)$. While the amplitudes of the modal phases are different at the two depths, undergoing a relative sign change every other mode, the magnitudes are approximately equal. The sign change can be compensated by a corresponding sign change in the modal phase vector $\underline{x}_k$, which may occur at another range, as seen in both Figures 1 and 2. For a "perfect" constant-index waveguide, in which the modes are sinusoidal, and the amplitudes go to zero at the bottom, the ambiguity is exact. In this special

case the modes are sinusoidal, given by $\sin(\frac{\pi d}{h}m)$. Now let us try to identify two depths d_1 and d_2 at which the magnitudes of the modes are equal. Equating the magnitudes yields

$$\sin^2(\frac{\pi d_1}{h}m) = \sin^2(\frac{\pi d_2}{h}m)$$
$$\rightarrow \cos(\frac{2\pi d_1}{h}m) = \cos(\frac{2\pi d_2}{h}m). \qquad (5)$$

Using the fact that discrete-time sinusoidal signals of the form $\exp(i\omega m)$ are the same for frequencies ω that are separated by an integer multiple of 2π, we have the following solution:

$$\frac{2\pi d_1}{h} \pm \frac{2\pi d_2}{h} = 2\pi \quad \rightarrow \quad d_1 = d_2 - h. \qquad (6)$$

Thus depth values that are symmetric about the the middle of the water channel are potentially ambiguous. The ambiguous depth shown in Figure 3, $\sim 83.5m$, is a little bit deeper that the depth predicted by Equation 6, $80m$, since a more realistic "soft" boundary condition is used that causes the eigenmodes to be non-zero in the sediment bottom, and also decreases their vertical wavenumbers, "stretching" them slightly.

4. STATE MODEL FOR TARGET MOTION

We wish to accommodate target motion, and discard the presumption of stationarity of the replica vector used in obtaining the Bartlett processor ($\underline{s}_k = \underline{s}$). We accommodate motion by using a hidden state process, where the state is given by the modal phases $\underline{x}_k$ of Equation 2:

$$\underline{x}_k = \mathbf{A}(\dot{r})(\underline{u}_k \odot \underline{x}_{k-1}). \qquad (7)$$

Here the state transition matrix $\mathbf{A}(\dot{r})$ is a diagonal matrix of phase factors, with the mth element being given by $\exp(-j\,k_r(m)\cdot\dot{r}\Delta t)$, where $\dot{r}$ is range-rate/horizontal-velocity, and Δt is the time between snapshots. The initial phase vector $\underline{x}_0$ is unknown. So what is assumed known in this model is not the initial range of the target, but only the change in range, or range-rate. The state-noise vector $\underline{u}_k$ consists of small phase perturbations. Its purpose is primarily to relax slightly the constraint imposed on the state sequence by the presumed horizontal wavenumber $k_r(m)$, which may have errors.

Denote the data matrix having the first k data vectors as its columns by $\mathbf{Y}_k$. Our goal is then to update the cumlative likelihood of the data, given a depth and range-rate pair $f(\mathbf{Y}_k|\dot{r}, d)$, as we acquire new data vectors $\underline{y}_k$. If the state vectors and the measurement vectors were both Gaussian, with linear transition matrices, then we could apply the expressions of Kalman filtering. The Kalman filter equations

provide expressions for a state prediction, measurement prediction, and state update; these are the conditional means of the densities $f(\underline{x}_k|\mathbf{Y}_{k-1})$, $f(\underline{y}_k|\mathbf{Y}_{k-1})$, and $f(\underline{x}_k|\mathbf{Y}_k)$. The Kalman equations also yield expressions for the error covariances associated with the estimates, which are the covariances of the three densities. The conditional means and covariances are then enough to characterize the densities, since the densities are Gaussian. So rather than viewing the Kalman filter as merely updating state estimates, we can view it as updating these densities, needed in turn to update the likelihood. In standard applications of Kalman filtering, parameters of interest, such as target range and velocity, comprise the state vector, and state estimates will suffice. In the application discussed here, the state consists largely of nuisance parameters; the parameters of interest must be inferred from the cumulative likelihood function $f(\mathbf{Y}_k|\dot{r}, d)$ estimated from approximations to these densities.

5. SEQUENTIAL RESAMPLING FOR STATE ESTIMATION

In lieu of an analytic expression for the updated likelihood, we employ a method of sequential resampling [4, 5]. This represents the densities parametrically, by a collection of samples, known as "particles." Loosely, we can think of the method as evolving histograms of samples, rather than analytic density expressions. The process is as follows [4]: at time-step k, we have some (prediction) samples $\underline{x}_k^{*(i)}$ which are distributed as $f(\underline{x}_k|\mathbf{Y}_{k-1})$. The first step is to scale, or weight, these samples according to the likelihood of the kth data snapshot. The weights are proportional to this likelihood, and normalized to sum to one:

$$w_k^{(i)} = \frac{f(\underline{y}_k|\underline{x}_k^{*(i)})}{\sum_i^N f(\underline{y}_k|\underline{x}_k^{*(i)})}. \qquad (8)$$

For our application, the likelihood was obtained by substituting Equation 2 into Equation 4. In the second step, the samples are resampled with a probability given by the likelihood, to yield a new set of (update) samples $\underline{x}_k^i$, which are distributed as $f(\underline{x}_k|\mathbf{Y}_k)$:

$$\text{Prob}\left[\underline{x}_k^{(j)} = \underline{x}_k^{*(i)}\right] = w_k^{(i)}. \qquad (9)$$

After this step, one typically has a significant number of samples $\underline{x}_k^i$ that are identical/degenerate, since they correspond to prediction samples $\underline{x}_k^{*(i)}$ that have high weight values. In the third step, the samples are translated according to the state transition equation, and state noise is added . This produces new prediction samples:

$$\underline{x}_{k+1}^{*(i)} = a(\underline{x}_k^{(i)}, \underline{u}_k^{(i)}) \qquad (10)$$

(the state noise $\underline{u}_k^{(i)}$ has the side effect of differentiating degenerate samples). One approach is to run separate estimators, or "particle filters," in parallel, one for every hypothesized range-rate and depth $(\dot{r}, d)$. Then the likelihood for each $(\dot{r}, d)$ pair can be approximated as follows:

$$
\begin{aligned}
f(\underline{y}_k|\mathbf{Y}_{k-1};\dot{r},d) &= \int d\underline{x}_k f(\underline{y}_k|\underline{x}_k;\dot{r},d) f(\underline{x}_k|\mathbf{Y}_{k-1};\dot{r},d) \\
&\simeq \sum_i^N f(\underline{y}_k|\underline{x}_k^{*(i)};\dot{r},d).
\end{aligned} \tag{11}
$$

And the cumulative likelihood is given by

$$
f(\mathbf{Y}_k|\dot{r},d) = \prod_{k=0}^N f(\underline{y}_k|\mathbf{Y}_{k-1};\dot{r},d). \tag{12}
$$

In practice, running parallel particle filters is likely to be computationally prohibitive. For example, 100 grid points in both depth and range would require 10,000 parallel estimators, each requiring a set of samples to represent the likelihood.

An alternative approach is to include the parameters of interest, in this case $(\dot{r}, d)$, in the state vector, with a uniform prior. Then an ambiguity surface may be obtained by plotting the marginal histogram of the update samples $\underline{x}_k^{(i)}$, which are distributed as $f(\underline{x}_k|\mathbf{Y}_k)$. The marginal histogram gives an approximation to $f(\dot{r}, d|\mathbf{Y}_k)$, which with a uniform prior on $(\dot{r}, d)$ is proportional to the likelihood $f(\mathbf{Y}_k|\dot{r}, d)$. A difficulty of this approach in practice is that the sequential resampling techniques tend to display the behavior of competitive dynamical systems (see, for example, [10]). That is, even if two sample regions have an equal level fitness with respect to the likelihood, over time one of them will tend to "win", and monopolize the samples. In our investigation we observed that with a target at 20m, some trials would show a peak at 20m, while other trials would show a peak at the depth ambiguity of 83.5m. So the ambiguity surface of a single trial does not reflect the intrinsic ambiguity over the ensemble of trials; it gives an over-optimistic picture of the ambiguity surface, and misleading in this respect.

To alleviate this problem, we chose a hybrid approach, putting velocity in the the state vector, but leaving depth, which we treat as the parameter of primary interest, out of the state vector. This requires a separate particle filter for each hypothesized depth. We chose 100 grid points in depth, leading to 100 corresponding particle filters. The histogram of particles at each depth provides an estimate of $f(\dot{r}|\mathbf{Y}_k, d)$. At each depth, we can use the equivalent of Equation 12 in order to obtain the likelihood:

$$
f(\mathbf{Y}_k|d) = \prod_{k=0}^N f(\underline{y}_k|\mathbf{Y}_{k-1};d). \tag{13}
$$

Assuming a uniform prior on d, then normalizing this with respect to d provides an estimate of $f(d|\mathbf{Y}_k)$. We can then compute an ambiguity surface as

$$
f(\dot{r}, d|\mathbf{Y}_k) = f(\dot{r}|\mathbf{Y}_k, d) \cdot f(d|\mathbf{Y}_k). \tag{14}
$$

Again, with a uniform prior on $(\dot{r}, d)$, this posterior density is proportional to the likelihood $f(\mathbf{Y}_k|\dot{r}, d)$.

To combat the problem of degeneracy of samples we implemented an approach suggested in [4]. Namely, in the state prediction step, additional state noise was added to differentiate degenerate samples. Since range-rate $\dot{r}$ was included in the state, noise was added to the range-rate values, with a standard deviation of 0.2 m/s. In addition, the 5% of the samples with the largest weights were automatically retained for the next step, to mitigate against losing a sample value on the basis of a single snaphot only.

6. SIMULATION AND RESULTS

Figures 4 and 5 show two ambiguity surfaces obtained in this manner, for a surface and submerged target, respectively. The SNR per sensor element was set at 0 dB. At each hypothesized depth we ran a particle filter with 500 samples or "particles". Depth estimates were obtained by taking the maximum of $f(\mathbf{Y}_k|d)$. Histograms of depth estimates for a surface target, obtained from 100 trials of the Bartlett estimator and the MTDE estimator, are shown in Figure 6. Similar histograms are shown for a submerged target at a depth of 20m in Figure 7. Note the ambiguity at a depth of about 83.5m. Because we run parallel particle filters for all hypothesized depths, the ambiguity surface for a single trial of the MTDE estimator, as in Figure 5, diplays this ambiguity.

To investigate the robustness of the estimators with respect to environmental uncertainty, the probability of correct localization (PCL) of the target is plotted versus increasing environmental uncertainty in Figure 8. The region of correct localization includes $\pm 2m$ around the true target depth, and around the depth ambiguity. As discussed in Section 3, the vertical wavenumbers in the estimator were perturbed by a uniform random variable whose range is expressed as a fraction of $\frac{\pi}{h}$. The PCL is plotted as this fraction is increased from 0 to 1.5. This environmental perturbation does not significantly degrade the localization of the surface target, but it does degrade the localization of the submerged target. The degradation is not as severe for the MTDE estimator as it is for the Bartlett estimator.

7. CONCLUSIONS

In this paper we have investigated an approach of joint estimation of range-rate and depth, rather than range and depth. Range-rate provides another dimension with which to discriminate targets against interfering sources (such as moving ships). In addition, discrimination based on range-rate is more robust with respect to environmental uncertainties, as verified by simulations. In lieu of an analytic expression of the updated likelihood, we have investigated a technique of sequential resampling or particle filtering. The limitation of this particular technique seems to be its ability to compensate for low SNR by integrating over many snapshots. It should be emphasized, however, that this is a limitation of the particle-filter implementation investigated here, and not a limitation of the basic state-model approach of localizing with respect to range-rate and depth, rather than range and depth. Our future work will be focused on implementations that more effectively exploit the entire data history.

8. REFERENCES

[1] J. L. Krolik, "Robust matched-field beamforming with benchmark shallow-water acoustic array data," in *1996 IEEE International Conference on Acoustics, Speech, and Signal Processing*, Atlanta, GA, May 1996.

[2] L. M. Zurk, N. Lee, J. Ward, and A. Gronosky, "Adaptive matched field processing for a moving target in a noisy shallow water channel," in *Proceedings of the 8th annual workshop on Adaptive Sensor and Array Processing*, Lexington, MA, March 2000, MIT Lincoln Laboratory.

[3] A. B. Baggeroer, W. A. Kuperman, and P. N. Mikhalevsky, "An overview of matched field methods in ocean acoustics," *IEEE J. of Oceanic Engineering*, vol. 18, no. 4, pp. 401–424, 1993.

[4] N. J. Gordon, D. J. Salmond, and A. F. M. Smith, "Novel approach to non-linear/non-gaussian bayesian state estimation," *IEE Proceedings-F*, vol. 140, no. 2, pp. 107–113, 1993.

[5] J. Liu and M. West, "Combined parameter and state estimation in simulation-based filtering," in *Sequential Monte Carlo Methods in Practice*, A. Doucet et al, Ed. Springer-Verlag, 2000.

[6] F. B. Jensen, W. A. Kuperman, M. B. Porter, and H. Schmidt, *Computational Ocean Acoustics*, American Institute of Physics Press, 1994.

[7] C. S. Clay and H. Medwin, *Acoustical Oceanography: Principles and Applications*, John Wiley and Sons, 1997.

[8] P. Stoica and R. Moses, *Introduction to Spectral Analysis*, Prentice Hall, 1997.

[9] S. Kraut, *Matched and Adaptive Subspace Detectors: Properties and Optimalities, and Statistical Analysis by a Method of Stochastic Representations*, Ph.D. thesis, University of Colorado at Boulder, 1999.

[10] J. Hofbauer and K. Sigmund, *Evolutionary Games and Population Dynamics*, Cambridge Univ. Press, 1998.
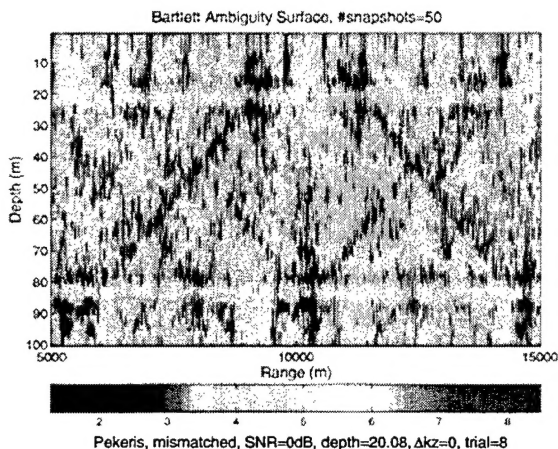
Figure 1: Bartlett estimator on moving target with perfectly known environment.
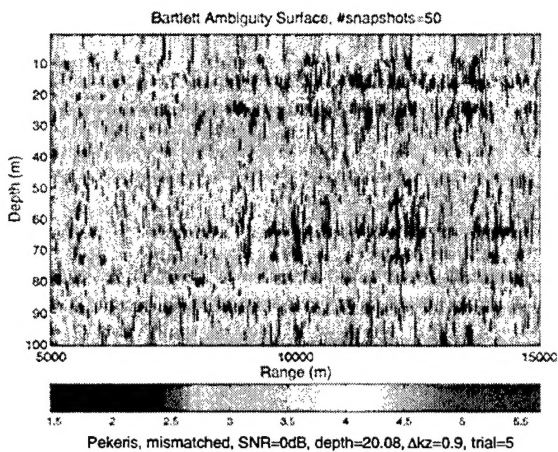

Figure 2: Bartlett estimator on moving target with mismatch in vertical wavenumbers in the range $[0, 0.9 \frac{pi}{h}]$.
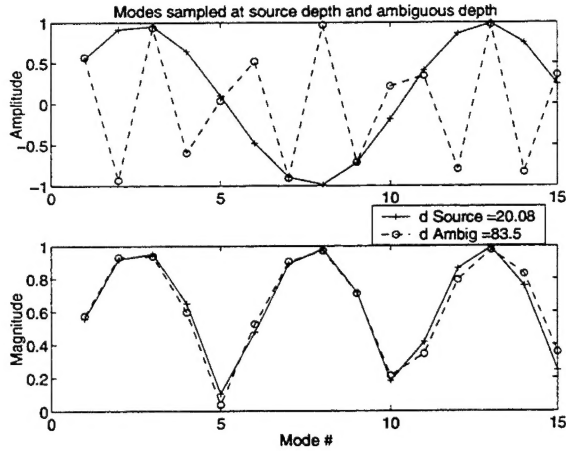
Figure 3: Modes at two ambiguous depths: (a) their amplitudes, and (b) their magnitudes.
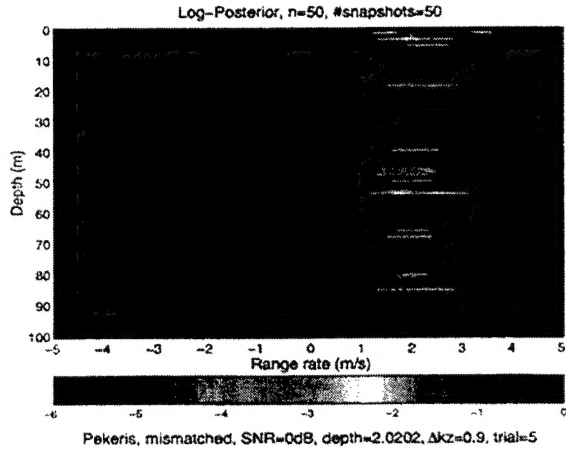

Figure 4: MTDE estimator: depth/range-rate ambiguity surface for a surface target.
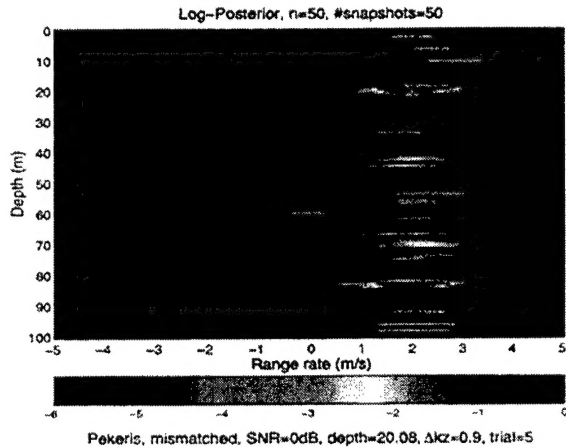

Figure 5: MTDE estimator: depth/range-rate ambiguity surface for a submerged target.
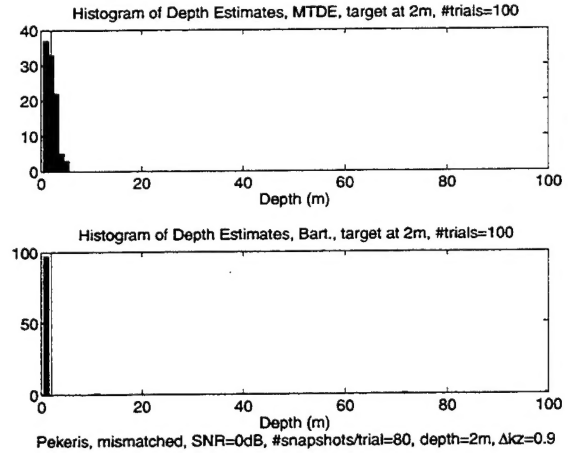

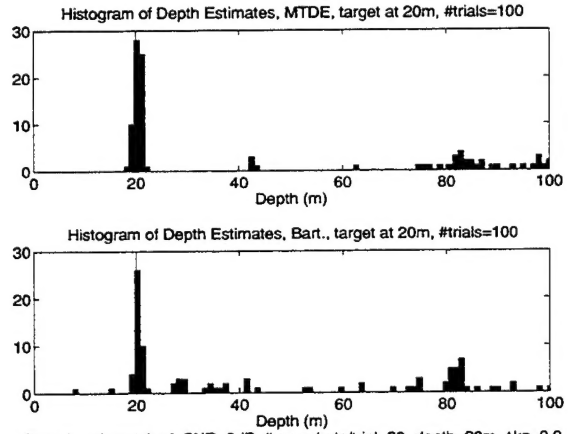Figure 6: Histograms of depth estimates for a surface target.

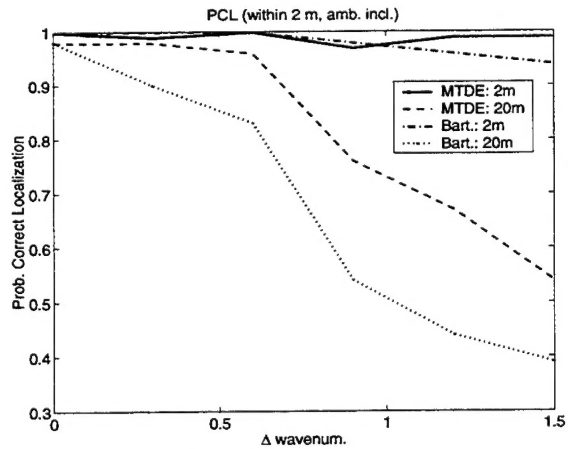Figure 7: Histograms of depth estimates for a submerged target.

Figure 8: Probability of correct localization for Bartlett and MTDE estimators, on both surface and submerged targets.

96